ARTICLES

The Role of Long-Range Forces in the Determination of Translational Kinetic Energy Release. Loss of $C_4H_4^+$ from the Benzene and Pyridine Cations

E. Gridelet,† R. Locht, A. J. Lorquet, J. C. Lorquet, and B. Leyh*

Department of Chemistry, University of Liège, Sart-Tilman (B6), B-4000 Liège 1, Belgium

Received: April 17, 2008; Revised Manuscript Received: July 24, 2008

Kinetic energy release distributions (KERDs) for the benzene ion fragmenting into $C_4H_4^+$ and C_2H_2 have been recorded by double-focusing mass spectrometry in the metastable energy window and by a retarding field experiment up to an energy of 5 eV above the fragmentation threshold. They are compared with those resulting from the HCN loss reaction from the pyridine ion. Both reactions display a similar variation of the kinetic energy release as a function of the internal energy: the average release is smaller than statistically expected, with a further restriction of the phase-space sampling for the $C_5H_5N^+$ dissociation. Ab initio calculations of the potential-energy profile have been carried out. They reveal a complicated reaction mechanism, the last step of which consists in the dissociation of a weakly bound ion−quadrupole or ion−dipole complex. The KERDs have been analyzed by the maximum entropy method. The fraction of phase space effectively sampled by the pair of fragments has been determined and is similar for both dissociations. Both reactions are constrained by the square root of the released translational energy, $\varepsilon^{1/2}$. This indicates that in the latter stage of the dissociation process, the reaction coordinate is adiabatically decoupled from the bath of the bound degrees of freedom. For the $C_6H_6^+$ fragmentation, the analysis of the experimental results strongly suggests that, just as for a spherically symmetric interaction potential, the translational motion is confined to a plane. For the dissociation of the pyridine ion, the main dynamical constraint is also a restriction to a two-dimensional subspace. This dimensionality reduction of the translational phase space is due to the fact that the Hamiltonian of both weakly bound complexes contains a cyclic coordinate.

1. Introduction

In the study of unimolecular reaction dynamics by statistical methods,[1−4] it is essential to distinguish between the analysis of rate constants and that of product energy distributions. In the particular case of dissociations taking place in an ion beam, a variety of experimental techniques are available to measure translational kinetic energy release distributions (KERDs) relatively easily and accurately.[5,6]

The conventional view[1] is that the calculation of a rate constant by transition state theory requires consideration of the properties of the system at short values of the reaction coordinate, up to the transition state only. By contrast, the analysis of product energy distributions, especially of KERDs, requires consideration of the long-range dynamics, that is, beyond the transition state (if any).

During the past few years, our group has argued[7−9] that an analysis of KERDs by the maximum entropy method (MEM)[10−12] is a powerful tool to investigate unimolecular dynamics and provides complementary information to a fit of the rate constant by a Rice−Ramsperger−Kassel−Marcus (RRKM) equation.[1−4]

However, our previous investigations have mainly focused on simple bond cleavage reactions. The halogen loss reaction of the bromo- and iodobenzene cations[13,14] as well as the hydrogen loss reactions from the benzene[15] and toluene[16] cations have been extensively studied. We now wish to examine more complicated dissociations leading to the release of molecular fragments. Two similar reactions have been selected,

$$C_6H_6^+ \rightarrow C_4H_4^+ + C_2H_2 \qquad (1.1)$$

and

$$C_5H_5N^+ \rightarrow C_4H_4^+ + HCN \qquad (1.2)$$

which both require a substantial rearrangement.

We have the following questions in mind.

(i) To what extent is the KERD influenced by preliminary rearrangements occurring before the dissociation itself?

(ii) It is usually assumed that the KERD reflects the details of the potential-energy surface after passing through the transition state.[1] But how is this to be interpreted when there is no saddle point during the last stretch of the reaction coordinate, that is, no reverse-activation-energy barrier?

(iii) Furthermore, at very large values of the reaction coordinate, the interaction can be expressed as a multipolar expansion of the interfragment potential. In the pyridine dissociation, $C_4H_4^+$and HCN are linked by a charge−permanent-dipole interaction. In the benzene dissociation, the leading term of the expansion is a charge−quadrupole interaction that links $C_4H_4^+$ and C_2H_2. Moreover, the anisotropic dependences differ for reactions 1.1 and 1.2. Is this difference in the long-range forces reflected in the KERD?

* Corresponding author: Fax: 32 4 366 34 13. E-mail: Bernard.Leyh@ulg.ac.be

† Formerly at the University of Liège; now at the NXP-TSMC Research Center, Kapeldreef 75, 3001 Leuven, Belgium.

10.1021/jp8033424 CCC: $40.75
Published on Web 09/19/2008

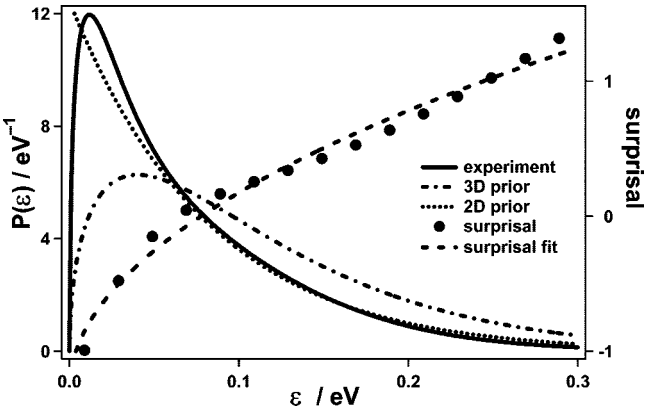

Figure 1. Comparison of the experimental KERD (solid line) to the 2-dimensional (dotted line) and 3-dimensional (dash-dotted line) prior distributions for the $C_6H_6^+ \rightarrow C_4H_4^+ + C_2H_2$ reaction studied in the metastable time window. The surprisal calculated with respect to the 3-dimensional prior distribution (eq 5.2) is also displayed (full circles, to be read on the right scale) and fitted to a $\lambda_0 + \lambda_1\varepsilon^{1/2}$ law (dotted line).

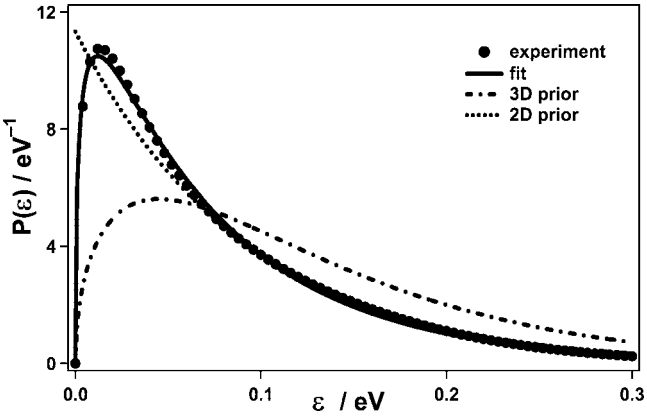

Figure 2. Fit (solid line) of the experimental KERD (full circles) obtained by using the MEM for the $C_6D_6^+ \rightarrow C_4D_4^+ + C_2D_2$ fragmentation recorded in the metastable time window. The 2-dimensional (dotted line) and 3- dimensional (dash-dotted line) prior distributions are also plotted for comparison.

Previous experimental results are available for reaction 1.2.[9,17] Reaction 1.1 has been extensively studied before. Its experimental rate constant is properly accounted for by the RRKM theory.[18−23] This result has been taken as evidence that the dissociation is statistical. The energy profile along the reaction coordinate of reaction 1.1 has been determined: ab initio calculations[24] have shown that the reaction mechanism is very complicated. It involves a sequence of extensive rearrangements that lead to the generation of a $C_4H_4^+$ ion that is generally thought to have a methylene cyclopropene structure, at least at the dissociation threshold.[9,25]

In the present paper, new experimental data on the fragment energy distributions for reaction 1.1 are reported, compared with those of reaction 1.2, and analyzed by the MEM with the help of ab initio calculations. The experimental techniques and the data handling procedures are outlined in Section 2. The essential relevant thermochemical issues are critically discussed in Section 3. The MEM is briefly described in Section 4 and is applied to our experimental results in Section 5. Ab initio calculations of the reaction mechanisms are reported in Section 6. A general discussion is given in Section 7. Conclusions then follow.

2. Experiment

The KERD, denoted as $P(\varepsilon|E)$, is the probability of releasing a kinetic energy ε on the dissociation fragments if E is the excess energy with respect to the dissociation asymptote. Both spectrometers used to measure it in specific energy ranges have already been described in previous publications,[26] and only the most salient features are reminded here. The experimentally recorded KERD is an average over the internal energy distribution of the parent ion, which depends on the kind of spectrometer used and on the experimental working conditions. This average KERD is noted $\tilde{P}(\varepsilon)$.

A. Metastable Dissociations. The experimental setup used to sample the metastable energy range is a two-sector forward geometry instrument; that is, the electrostatic analyzer is followed by the magnet. The internal energy sampled, E, depends on the dissociating ion but is usually in the 0.5−1.2 eV range above the dissociation asymptote. Parent ions are produced upon electron impact in the spectrometer source and then accelerated by a voltage difference V_{acc}. Scanning V_{acc}, with fixed electric and magnetic fields, leads to a mass spectrum of parent ions dissociating to a given fragment ion in the first field-free region of the spectrometer.[27−29] In this ion kinetic-energy spectrum measured in the laboratory reference frame, peaks are broadened by the kinetic energy released during the fragmentation. Because the residual pressure in the field-free region is in the 10^{-8} mbar range, collision-induced processes may be ignored.

KERDs are deduced from the experimental peak shape by a differentiation procedure followed by a change of variables from the laboratory to the center-of-mass reference frame.[6,30,31] Because the peak width is equal to about 50 eV in the laboratory reference frame compared to a translational energy of the center-of-mass of about 7.5 keV in the direction of the spectrometer optical axis, angular discrimination effects may be neglected. Otherwise, they could be taken into account by a more elaborate procedure.[32−34] A deconvolution step is included in the data handling in order to remove the broadening by the experimental apparatus function.[16]

Benzene (commercially available from Merck with 99.9% purity) and benzene-d_6 (available from Aldrich with 98% stated purity) were used without further purification. In the spectrometer source, the kinetic energy of the ionizing electron is equal to 70 eV, and the emission current is set at 10 μA. The accelerating voltage V_{acc} is scanned around 7.5 kV. The electrostatic analyzer exit slit (β-slit) width is adjusted to 0.25 mm to reach a translational energy resolution $\Delta E/E$ of 10^{-3}.

Fragmentations taking place in the spectrometer first field-free region occur in a time window characterized by the entrance time (τ_1) into and by the exit time (τ_2) out of this region. Through the rate constant $k(E)$, this time selection is equivalent to the selection of a relatively narrow range of internal energies. Accordingly, the internal-energy distribution of the parent ions is given by the product of a transmission function, $T(E)$, that depends on the rate constant $k(E)$,[20,23,35−37] and of the branching ratio $R(E)$[38] corresponding to the selected dissociation channel (here, $C_4H_4^+ + C_2H_2$), that is, the ratio between the ion current for the fragment of interest and the total ion current at internal energy E

$$T(E) = A[\exp(-k(E)\tau_1) - \exp(-k(E)\tau_2)]R(E) \quad (2.1)$$

where A is a normalization constant.

B. Photoionization/Retarding Field Analysis. This technique provides access to a more extended internal energy range of a few electron Volts.[26,39] The sample, introduced by effusion

in a reaction chamber, is ionized by photons emitted by a rare-gas discharge lamp. The resonance lines Ne(I) (16.67−16.85 eV) and He(I) (21.21 eV) were used in the present case, so that internal energies up to a few electron Volts can be accessed. Photoelectron spectra are recorded by a Lindau-type electron energy analyzer, and ions ($C_6H_6^+$ or $C_4H_4^+$) are analyzed by an ion-retarding potential device, followed by a quadrupole mass spectrometer. The measurement principle is that only ions with enough kinetic energy are able to surmount the retarding-potential barrier and are thus detected. Therefore, by scanning the retarding potential while focusing on a given fragment ion, the kinetic energy of which is denoted ε_f, one gets a retarding curve, $I(\varepsilon_f)$: its derivative leads then to the kinetic energy distribution. Taking into account the fact that angular discrimination affects high kinetic energy ions, the relationship between the retarding curve and the ion translational energy distribution $\tilde{P}(\varepsilon_f)$ has been shown to be:

$$\tilde{P}(\varepsilon_f) \propto \varepsilon_f^{\mu} \frac{dI(\varepsilon_f)}{d\varepsilon_f} \tag{2.2}$$

where $\mu = 0.43 \pm 0.03$.[39] For every measurement, fragment-ion and parent-ion retarding curves have been recorded sequentially.

The internal energy distribution, $T(E)$, of the $C_6H_6^+$ ions that dissociate via reaction 1.1 is given by the He(I) or Ne(I) photoelectron spectrum multiplied by the branching ratio, $R(E)$, for the selected dissociation channel.[38]

In such retarding field experiments, the thermal energy of the parent ion provides a non-negligible contribution to the fragment kinetic energy, and a deconvolution step is compulsory.[9] The velocities corresponding to the thermal motion [with a distribution $\tilde{P}^T(\mathbf{v})$] and to the kinetic energy released [with a distribution $\tilde{P}^{KER}(\mathbf{v})$] are vectorially added to give the observed fragment velocity [with a distribution $\tilde{P}^f(\mathbf{v})$]. For this reason, the deconvolution procedure must consider the velocity vectors and not the kinetic energies.

$$\tilde{P}^f(\mathbf{v}) = \tilde{P}^T \otimes \tilde{P}^{KER}(\mathbf{v}) \tag{2.3}$$

The thermal distribution $\tilde{P}^T(\mathbf{v})$ is obtained by a fit of the parent-ion retarding curve based on a Maxwell velocity distribution

$$\tilde{P}^T(\mathbf{v}) \propto \exp(-\alpha_T v^2) \tag{2.4}$$

To proceed further, we need an analytical form for $\tilde{P}^{KER}(\mathbf{v})$. As detailed in Section 4, the maximum entropy formalism provides us with a suitable analytical form for $\tilde{P}(\varepsilon)$ (eq 4.3 after averaging over $T(E)$) and thus also for $\tilde{P}^{KER}(\mathbf{v})$. This form depends on constraints A_i and associated Lagrange multipliers λ_i. It can be shown that these constraints and multipliers can be determined by fitting the following equation to the experimental data

$$\tilde{P}^f(v;\lambda_i,A_i) = (N_f/v)\int_0^{\infty} v' \sinh(2\alpha_T v v') \times \exp[-\alpha_T(v^2+v'^2)]\tilde{P}^{KER}(v';\lambda_i,A_i)\, dv' \tag{2.5}$$

where N_f is a normalization factor. Once these parameters have been obtained, the deconvoluted distribution, expressed in terms of kinetic energy, can be easily reconstructed by using eq 4.3.

The results for the pyridine fragmentation studied by the retarding-field experiment have already been published,[9] but they were flawed by a small mistake in the deconvolution procedure. In rectifying them, it appeared that the correction does not affect the validity of our previous discussion. Note that the procedure was already put right in our following publications.[15,40] The corrected experimental results are displayed in the present article, together with the benzene results.

3. Thermochemistry

Does $C_4H_4^+$ formation from either the benzene or the pyridine cations involve a reverse activation barrier? Two experimental pieces of information are briefly reviewed: appearance-energy data and KERDs.

A. $C_5H_5N^+ \rightarrow C_4H_4^+ + HCN$. Appearance-energy measurements have been performed by various groups, extending from the microsecond[41,42] up to the millisecond time range.[43−46] From all available data, we adopt a 0 K threshold of 12.1 ± 0.1 eV as a cautious conclusion.

Burgers et al.[47] have shown by neutralization−reionization mass spectrometry that the neutral moiety has the H−C≡N structure. There seems to be a consensus that the $C_4H_4^+$ ions produced upon fragmentation of many precursors consist of a mixture of the methylenecyclopropene (MCP) and the vinylacetylene (VA) isomers.[48] The population ratio is 68:32 for the $C_6H_6^+$ fragmentation, but no such data have been reported for $C_5H_5N^+$. On the basis of photoelectron spectroscopy results,[25] known thermochemical[49] and vibrational spectroscopy data,[50] as well as recent G3 level ab initio data,[51] a threshold of 12.0 eV can be calculated for $MCP^+ + HCN$, in good agreement with the 0 K appearance-energy data. We therefore conclude that $C_4H_4^+$ is produced in the MCP geometry at its thermochemical threshold. If any reverse activation barrier exists, its height should be limited to ∼0.1 eV.

Arakawa et al.[46] also estimated the average kinetic energy released, $\langle\varepsilon\rangle$, from the width at half maximum of the metastable peaks. $\langle\varepsilon\rangle$ displays a clear trend toward zero as the lifetime of the metastable ions increases, suggesting that there is no reverse activation barrier.

B. $C_6H_6^+ \rightarrow C_4H_4^+ + C_2H_2$. The situation is less convincing for the dissociation of the benzene cation than for that of the pyridine cation. The available appearance energy measurements span a wide range: from 13.38 eV[36] to 14.22 eV.[38] The most recent threshold, determined by Holland et al. by using time-of-flight mass spectrometry is equal to 14.22 eV.[38] These authors interpret this relatively high appearance energy as corresponding to the production of the VA cation, stating that cyclic $C_4H_4^+$ fragments would be produced at lower energy. It is, however, unclear why the most abundant isomer, ionized MCP, would give rise only to a vanishingly small signal below 14.2 eV. In addition, with a flight time in the microsecond range, a kinetic shift of a few tenth of an electron Volt can be predicted.[36] Our own recent measurements by quadrupole photoionization mass spectrometry lead to an appearance energy of 13.93 ± 0.15 eV,[52] a value also affected by a kinetic shift. According to Neusser,[36] a rate constant of 500 s^{-1} corresponds to this appearance energy, which is compatible with our detection sensitivity. Neusser's rate constant measurements combined with RRKM modeling lead to a threshold of 13.38 eV,[36] which can be assigned to the production of the most stable MCP ionized isomer. The difference between 14.22 and 13.38 eV, that is, 0.84 eV, is, however, about twice the calculated isomerization energy relating the MCP and the VA cations,[9,53,54] which again pleads against Holland's assignment. The extrapolation procedure performed by using the RRKM equation, which, in principle, accounts for the kinetic shift, might, however, not be reliable enough for our purpose because the measured data cover only the microsecond range.

On the basis of available data,[25,49] the thermochemical threshold for the $MCP^+ + C_2H_2$ fragments is estimated at 13.54

eV, suggesting the absence of any reverse activation barrier. The ab initio calculations of van der Hart[24] lead to a reverse barrier of 0.09 eV. In addition, as discussed in the next sections, the analysis of the KERDs by the MEM indicates that no reverse activation energy needs to be introduced to account for the experimental data.

4. Maximum Entropy Method

Consider a unimolecular dissociation where the ergodic assumption is perfectly fulfilled, that is, where all quantum states at total energy E are equally probable. The probability of observing a given kinetic energy release ε is proportional to the number of quantum states that give rise to this particular value of the kinetic energy. Therefore, the corresponding KERD, termed the prior distribution $P^0_{3D}(\varepsilon|E)$, is provided by the density of states of a pair of fragments that separate with a relative translational energy ε at total energy E.[6−17]

$$P^0_{3D}(\varepsilon|E) = A(E)\varepsilon^{1/2}\rho_{int}(E-\varepsilon) \quad (4.1)$$

The subscript 3D serves as a reminder that the density of translational states, $\varepsilon^{1/2}$, has been calculated for a three-dimensional motion. $A(E)$ is a normalization factor, and ρ_{int} is the density of internal states (rotational and vibrational) of the fragments. The internal energy E is always measured with respect to the dissociation asymptote.

However, the experimental KERD, $P(\varepsilon|E)$, is in practice never identical to the prior distribution. The MEM relates their ratio to a certain number of dynamical constraints $A_i(\varepsilon)$ that prevent the reaction from being fully ergodic.[10−12]

$$P(\varepsilon|E) = P^0_{3D}(\varepsilon|E)\exp[-\lambda_0(E)]\exp[-\lambda_1(E)A_1(\varepsilon)]\times \exp[-\lambda_2(E)A_2(\varepsilon)]\ldots \quad (4.2)$$

where $\lambda_i(E)$ is the Lagrange multiplier conjugated to the constraint $A_i(\varepsilon)$. The quantity $\exp[-\lambda_0(E)]$ is a normalization constant. Fortunately, eq 4.2 often reduces to a single corrective factor:

$$P(\varepsilon|E) = P^0_{3D}(\varepsilon|E)\exp[-\lambda_0(E)]\exp[-\lambda_1(E)A_1(\varepsilon)] \quad (4.3)$$

The simplest way to identify the constraint is then to plot the surprisal

$$I(\varepsilon|E) = \ln[P^0_{3D}(\varepsilon|E)/P(\varepsilon|E)] = \lambda_0(E) + \lambda_1(E)\mathrm{A}_1(\varepsilon) \quad (4.4)$$

as a function of ε at a given value of E and to look for the analytical form of $A_1(\varepsilon)$ that correctly fits $I(\varepsilon|E)$.

The number of configurations in phase space that generate a given distribution is measured by the entropy S of the distribution. The entropy is thus maximum for the most statistical distribution, that is, for the prior distribution $P^0_{3D}(\varepsilon|E)$. The discrepancy between the experimental and the prior distributions is measured by the value of the entropy deficiency DS, which can be extracted from the experiment and which is inversely related to the efficiency of phase-space sampling.

$$\mathrm{DS}(E) = S[P^0_{3D}(\varepsilon|E)] - S[P(\varepsilon|E)]$$

$$= \int_0^E P(\varepsilon|E)\ln[P(\varepsilon|E)/P^0_{3D}(\varepsilon|E)]\,\mathrm{d}\varepsilon$$

$$= -\lambda_0(E) - \lambda_1(E)\langle A_1(\varepsilon)\rangle - \lambda_2(E)\langle A_2(\varepsilon)\rangle \quad (4.5)$$

A major interest of the concept of entropy deficiency is that it can be used to estimate the fraction of phase space effectively sampled by the pair of fragments.[55,56]

$$F(E) = \exp[-\mathrm{DS(E)}] = \exp[\lambda_0(E) + \lambda_1(E)\langle A_1(\varepsilon)\rangle + \ldots] \quad (4.6)$$

F is an index that is determined by the coupling between the reaction coordinate and the bath formed by the remaining oscillators: the stronger the coupling, the more ergodic the KERD and the higher the F index. Because restrictions to phase-space sampling that do not affect the kinetic-energy release are not taken into account in its definition, it provides an upper limit for the ratio between two volumes of phase space: that actually explored by the dissociating system and that in principle available at the total energy E.

A two-dimensional prior distribution, denoted $P^0_{2D}(\varepsilon|E)$, will also be used in our analysis. It corresponds to the most statistical planar motion and is especially appropriate when the interaction potential between fragments is spherically symmetric because the nuclear trajectories that generate the KERD are then constrained to be planar.[40,57] Because the density of translational states of a particle moving in a two-dimensional subspace is constant, eq 4.1 is now replaced by:

$$P^0_{2D}(\varepsilon|E) = A'(E)\rho_{int}(E-\varepsilon) \quad (4.7)$$

5. Results

A. Density of States. The density of states of the pair of fragments has been calculated by a Beyer−Swinehart direct-count method including rotation.[1,3] The required vibrational frequencies and rotational constants of the MCP ion are available from a previous calculation.[9] Actually, only two-thirds of the $C_4H_4^+$ fragments resulting from benzene ion fragmentations have the MCP geometry, the last third displaying the VA conformation.[48] However, as discussed in our earlier work,[9] the rate of increase of the density of states as a function of the internal energy is similar for the VA and the MCP ions. Therefore, the branching ratio between the two isomers of $C_4H_4^+$ has a negligible influence on the calculated prior distribution.

B. KERD and Surprisal Fit. The measured distribution $\tilde{P}(\varepsilon)$ for reaction 1.1 is an average of $P(\varepsilon|E)$ over the distribution function $T(E)$ defined in Section 2.

$$\tilde{P}(\varepsilon) = \int_\varepsilon^\infty P(\varepsilon|E)T(E)\,\mathrm{d}E \quad (5.1)$$

In the metastable window, $T(E)$ is fairly narrow. An average surprisal can be computed as

$$\tilde{I}(\varepsilon) = \ln[\tilde{P}^0_{3D}(\varepsilon)/\tilde{P}(\varepsilon)] \approx \lambda_0 + \lambda_1\mathrm{A}_1(\varepsilon) \quad (5.2)$$

where λ_0 and λ_1 are assumed to be independent of E. Figure 1 displays the metastable KERD for reaction 1.1 and the corresponding surprisal fit. For reactions 1.1 and 1.2 including also the perdeuterated species, $\tilde{I}(\varepsilon)$ is found to vary linearly with $\varepsilon^{1/2}$. This leads to the identification of $\mathrm{A}_1(\varepsilon)$ with $\varepsilon^{1/2}$. Figure 2 illustrates the good quality of the fits for reaction 1.1.

The retarding-field experiments involve a much broader range of internal energies: eq 5.2 is then no longer useful. The relationship between λ_1 and the total energy E has to be taken into account, but this function is a priori unknown. Two assumptions were tried[9] for the function $\lambda_1(E)$: either constant in the whole energy range or expressed as a linear function of E. Both choices lead to approximately the same value of λ_1 at the average internal energy of the parent ion, $\langle E\rangle$.

Furthermore, the measured retarding-field curves are the result of a convolution product that smoothes the shape of the

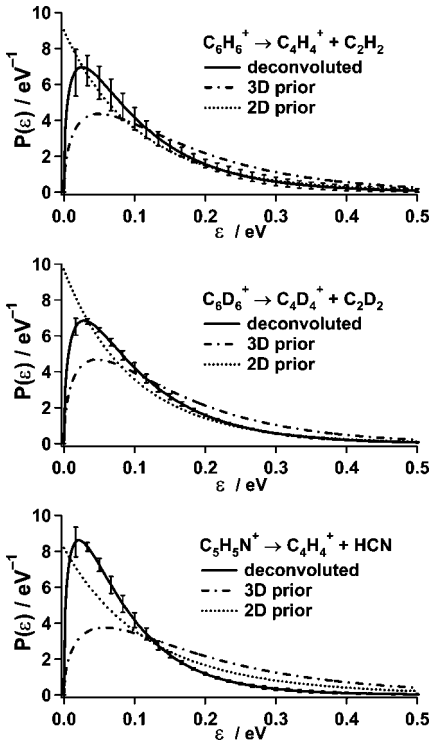

Figure 3. Solid lines with error bars: deconvoluted KERDs obtained by using the retarding-potential method with NeI excitation. The 2-dimensional (dotted line) and 3-dimensional (dash-dotted line) prior distributions are also displayed for comparison. Top: $C_6H_6^+ \rightarrow C_4H_4^+ + C_2H_2$. Middle: $C_6D_6^+ \rightarrow C_4D_4^+ + C_2D_2$. Bottom: $C_5H_5N^+ \rightarrow C_4H_4^+ + HCN$.

distribution. This smearing prevents us from discriminating between two possible assumptions for the constraint $A_1(\varepsilon)$: $\varepsilon^{1/2}$ or ε.

Altogether, the fits are very satisfactory. Figure 3 shows some examples of deconvoluted KERDs. They are narrower than the prior distribution. The error bars take into account both the experimental reproducibility and the uncertainty about the data handling procedure.

C. Average Kinetic-Energy Release and Efficiency of Phase-Space Sampling. Finally, the values of the average kinetic energy $\langle\varepsilon\rangle$ and of the index F are calculated at the energy $\langle E\rangle$ by averaging over all fits ($\lambda_1(E)$ constant or linear and $A_1(\varepsilon)$ equal to $\varepsilon^{1/2}$ or ε).

$\langle\varepsilon\rangle(E)$ for reaction 1.1 is displayed in Figure 4a along with the first moments of the three- and two-dimensional prior distributions (defined by eqs 4.1 and 4.7). The dynamics happens to generate less kinetic energy than expected statistically on the basis of a three-dimensional motion. The two-dimensional expectation is, however, close to the experimental findings. Few experimental data are available for comparison. From Jarrold's data[19] on benzene in the metastable window of the second field-free region of a ZAB-2F instrument, an average kinetic-energy release of 0.055 eV can be inferred at an internal energy E which we estimate (on the basis of their measured branching ratios) to lie around 0.7 eV. This agrees quite well with our own metastable data at somewhat smaller lifetimes: $\langle\varepsilon\rangle = 0.066$ eV at $E = 0.95$ eV. The data previously reported by Baer et al.[18] about the dissociations of two other $C_6H_6^+$ isomers (2,4 hexadiyne and 1,5 hexadiyne) into $C_4H_4^+$ and C_2H_2 show a similar trend but are offset by about +30 meV. They lie, however, clearly close to a canonical two-dimensional prior expectation, too (see Figure 5 of ref 18).

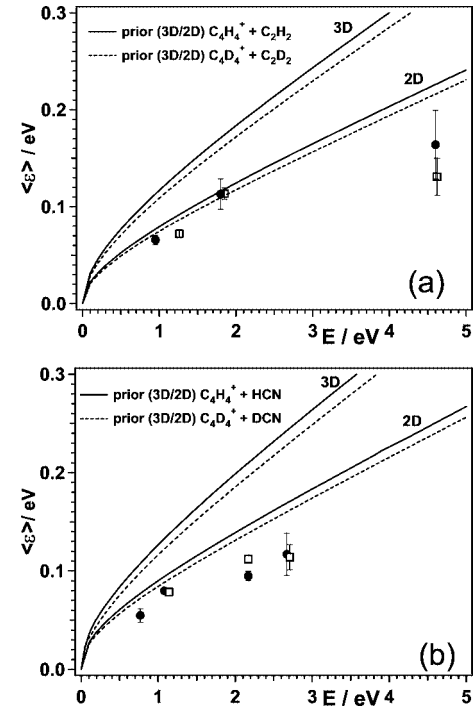

Figure 4. Average kinetic energy release in the metastable time window and obtained by using dissociative photoionization coupled with a retarding-field device compared with the 3- and 2-dimensional prior predictions (solid line: nondeuterated species; dashed line: perdeuterated species). Filled circles: undeuterated species; open squares: deuterated species. Top: dissociation of the benzene and perdeuterated benzene cations. Bottom: dissociation of the pyridine and perdeuterated pyridine cations.

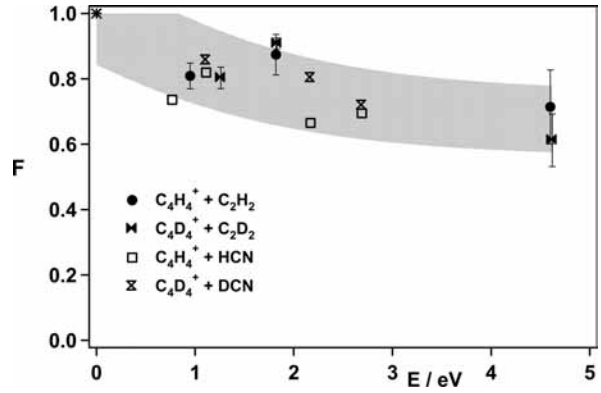

Figure 5. Evolution of the F index with internal energy for the $C_4H_4^+$ loss from ionized benzene and pyridine and their perdeuterated isotopomers. The gray area is a guide for the eye to highlight the global decrease of F. The star at ($E = 0$, $F = 1$) corresponds to the (nonmeasured) threshold situation where only one phase-space cell is available and is necessarily occupied.

The same data handling procedure has been used for the retarding-field curve of the pyridine dissociation (reaction 1.2).[9] The resulting data are displayed in Figure 4b. A strong similarity with the $C_6H_6^+$ dissociation emerges.

The fraction of phase space effectively explored, as measured by the index $F(E)$, is displayed in Figure 5. At threshold, F is necessarily equal to 1 because the accessible phase space reduces to one cell which must then be sampled. The grouping of the data obtained for the four reactions 1.1 and 1.2 including the perdeuterated species stresses the similarity between the behavior of benzene and pyridine ions. Despite an important scattering of the data points, $F(E)$ decreases monotonically as

E increases and reaches a value of about 80% at $E = 4.5$ eV. As already noticed in the case of the pyridine dissociation,[9] no isotope effect is detectable.

6. Ab Initio Calculations

A large number of ab initio calculations were undertaken in order to determine the lowest energy pathway for the formation of the $C_4H_4^+$ fragment and, especially, in order to check whether its formation from either the benzene or pyridine cation involves a reverse activation-energy barrier. Unfortunately, this turned out to be a very difficult task. An insight into the difficulties is given below.

The computations were carried out with the GAUSSIAN system of programs[58] by using basis sets of increasing size to ascertain the stability of the analysis. Density functional theory calculations performed by using the B3LYP functional were compared with quadratic configuration interaction calculations including single and double excitations (QCISD). (The meaning of the acronyms is explained in standard textbooks.[59]) The results were often disappointing because, as noted in a recent discussion[60] of the reliability of barrier-height calculations, there exists a "tendency of many density functionals to underestimate potential barriers [...] in contrast to ab initio methods, which tend to overestimate (them)". In many cases, the transition state of a rearrangement was found to lie below the dissociation asymptote when calculated at the B3LYP/6-31G(d) level. However, when the calculation was repeated at the (more accurate) QCISD level, the isomerization barrier was found to be higher than the asymptote, irrespectively of the size of the basis set of atomic orbitals.

Furthermore, when the reverse activation barrier is very small, the zero-point energy correction to be added is of decisive importance. However, the calculated vibrational frequencies of the transition state are often overestimated, because they are calculated as if the potential energy surface were harmonic in the neighborhood of the saddle point, which is not often the case.

Finally, we also detected an interconversion between $^2A'$ and $^2A''$ electronic states of the pyridine cation involving a conical intersection. For nonplanar geometries, the two electronic states belong to the same representation and the genuine crossing converts to a saddle point.

A. Benzene Cation. Multireference configuration interaction ab initio calculations with a 6-31G(d,p) basis set of atomic orbitals aiming at determining the lowest-energy pathway for the formation of the $C_4H_4^+$ fragment from the benzene radical cation have been carried out by van der Hart.[24] The last part of the reaction path was found to start from a stable $C_6H_6^+$ isomer having the structure of a charged MCP^+ conformation linked to an acetylene molecule. This structure evolves adiabatically to the fragments via a simple CC-bond stretching motion, in the course of which a transition state is next encountered along the reaction path, followed by a shallow minimum resulting from an ion-induced dipole interaction. van der Hart's calculations locate the energy of the last transition state 2 kcal mol^{-1} above that of the dissociation asymptote. This is probably an overestimate because of the unreliability of the zero-point energy correction. The transition state was found to be characterized by the existence of four equivalent conformations that easily interconvert via a very anharmonic force field.

Altogether, the picture that emerges is consistent with a complicated reaction mechanism, the last step of which consists of the dissociation of a weakly bound ion−quadrupole complex $MCP^+•C_2H_2$ by a simple CC-bond stretching motion without a reverse activation energy barrier. The stability of the complex was calculated by the QCISD/6-311G(d,p)//QCISD/6-31G(d) procedure and led to a value of 0.14 eV.

B. Pyridine Cation. A large number of calculations were attempted in order to determine the dissociation pathway of the pyridine ion.

Six different kinds of stable structures were detected: (i) the normal pyridine geometry, (ii) two six-membered rings with a hydrogen shift, presenting one carbon atom with no hydrogen and another one linked to two of them, (iii) a five-membered pyrrolic ring, (iv) an open chain having the $HC-N-CH-CH-C-CH_2^+$ structure (another much less stable open chain isomer was also detected), (v) an ion−ipole complex where an HCN molecule is loosely bound to a MCP^+ ion, and (vi) a similar weakly bound complex where HCN interacts with a VA ion.

Unfortunately, the complete reaction mechanism leading from the original pyridine structure to the lowest dissociation asymptote could not be reconstructed. No less than 21 transition states were found to connect these stable structures. Many of them describe numerous isomerization possibilities among floppy structures. Only the last step is secure: the ion−dipole complex $MCP^+•HCN$ dissociates without any reverse activation energy barrier. Its most stable structure is calculated at the QCISD/6-311G(d,p)//QCISD/6-31G(d) level to be 0.53 eV below the dissociation asymptote. (A value of 0.52 eV was derived from a QCISD/6-31++G(d,p)//QCISD/6-31G(d) calculation.) The nuclear framework belongs to the C_s point group, and the ground electronic state is $^2A''$. However, its structure is floppy because the potential-energy surface is very flat: the two moieties have considerable freedom to stroll about each other.

7. Discussion

The experimental results displayed in Figures 1−5 highlight three major pieces of information which will now be discussed in detail.

(i) Although reactions 1.1 and 1.2 require large structural rearrangements, their KERD shapes are not only similar to each other but also to those previously obtained for simple bond cleavage reactions leading to an atom loss.[13,14,17] Moreover, the dissociations of two $C_6H_6^+$ isomers (2,4-hexadiyne and 1,5-hexadiyne) into $C_4H_4^+$ and C_2H_2 behave similarly.[18] When a constraint can be unambiguously identified, it is found to be equal to the square root of the released translational energy, $\varepsilon^{1/2}$, as for simple-bond dissociations.[13,14,17] The average kinetic-energy release $\langle\varepsilon\rangle$ is lower than the value $\langle\varepsilon\rangle_0$ expected from the three-dimensional prior model.

(ii) A finer comparison between parts a and b of Figure 4 shows, however, that the pyridine cation behaves even less statistically than the benzene cation.

(iii) For the benzene ion dissociation 1.1, the two-dimensional prior distribution $P^0_{2D}(\varepsilon|E)$ is found to be in good agreement with the experimental KERD at least up to an internal energy of 3 eV (Figures 1, 2, 3, and 4a), even though the ion−quadrupole interaction potential between the receding fragments is not spherically symmetric. Even for the less statistical fragmentation of the pyridine cation, Figure 4b shows that the two-dimensional prior distribution is closer to the experimental data than the three-dimensional one.

We examine these three points in turn in the following discussion. We first show how the decoupling of the reaction coordinate from the internal degrees of freedom of the fragments accounts for the $\varepsilon^{1/2}$ constraint (Section 7.A) and for the sign

of λ_1 (Section 7.B). Not only the similarity between the KERDs of reactions 1.1 and 1.2 (point (i) above) but also their specificities (point (ii)) follow naturally from this MEM analysis, as shown in Section 7.C. In the last subsection (Section 7.D), an argument based on the classical Hamiltonian of a model system is presented to justify the dimensionality reduction (point (iii)) suggested by Figures 1−4.

A. Adiabatic Separation of the Reaction Coordinate. The commonly accepted view is that KERDs should provide information on the long-range dynamics.[1] Section 6 has emphasized that the last step of the fragmentation mechanism consists in a simple barrierless cleavage of a $MCP^+ \bullet C_2H_2$ or $MCP^+ \bullet HCN$ complex. However, the asymptotic expression of the interaction potential is very different for the two reactions studied here. The leading term in the expression of the long-range potential between $C_4H_4^+$ and C_2H_2 describes the charge-quadrupole interaction

$$V(r,\theta) = \frac{qQ}{2r^3}(3\cos^2\theta - 1) \tag{7.1}$$

where θ denotes the angle between the principal axis of the neutral fragment and the line joining both fragments, q is the charge of the ion, r is the interfragment distance, and Q is the quadrupole moment of acetylene. For the $C_4H_4^+ +$ HCN interaction, the leading term is the charge−permanent-dipole contribution

$$V(r,\theta) = -\frac{q\mu_D}{r^2}\cos\theta \tag{7.2}$$

where μ_D is the permanent electric dipole moment of hydrogen cyanide.

At large values of the separation coordinate r, the neutral fragment, either HCN or C_2H_2, undergoes free rotation in the field of the ion. As pointed out by Bates[61] and by Schlier,[62] the cyclic action integral $\oint p_\theta \, d\theta$, where p_θ is an angular momentum, is an adiabatic invariant of the problem; that is, the reaction coordinate is adiabatically decoupled from rotation. Recent research[63,64] has shown that the Poisson bracket of the adiabatic invariant is proportional to $p_r \mu r^{-3}$ for the ion−dipole interaction and to $p_r Q r^{-4}$ for the ion−quadrupole case. This short-range behavior of the Poisson bracket implies that the quality of the adiabatic approximation is expected to be quite good, at least at asymptotically large values of r. However, because it also increases linearly with the translational momentum p_r, the validity of the adiabatic separation becomes questionable at high translational energies.

When the reaction coordinate is adiabatically decoupled from the bath, the dynamics is equivalent to a one-dimensional motion along the reaction coordinate in an effective potential.[62−64] The equation of motion obeys Jacobi's form of the least-action principle, which is particularly simple when the dynamics is one-dimensional.[63−65] This principle asserts[57,66] that the actual trajectory between two points r_1 and r_2 minimizes the integral $\int_{r_1}^{r_2} \varepsilon^{1/2} \, dr$. This accounts[63−65] for the fact that, for both reactions 1.1 and 1.2, the dynamical constraint to be used in the MEM is $\varepsilon^{1/2}$, in conformity with the experimental findings at low internal energy (metastable domain, Figures 1 and 2).

B. Statistics and Dynamics. The MEM clearly distinguishes between the roles played by statistics and by dynamics in energy partitioning problems. At not too high internal energies at least, KERDs have been found to obey eq 4.3 with $A_1 = \varepsilon^{1/2}$ (Figures 1 and 2).

$$P(\varepsilon|E) = P^0_{3D}(\varepsilon|E)\, e^{-\lambda_0}\, e^{-\lambda_1 \varepsilon^{1/2}} \tag{7.3}$$

Note the physical meaning of each of the three factors. The statistical information is contained in the prior distribution P^0. The third factor, $\exp(-\lambda_1\varepsilon^{1/2})$, is a dynamical correction, and the middle one, $\exp(-\lambda_0)$, is a mere normalization constant.

Equation 7.3 accounts for the fact that, even though the long-range forces are very different, similarity in the KERD shapes for reactions 1.1 and 1.2 is to be expected. The reasons are as follows.

First, the prior distributions $P^0_{3D}(\varepsilon\,|E)$ of reactions 1.1 and 1.2 are similar. This results from the fact that the vibrotational degrees of freedom of HCN and of C_2H_2 form two roughly equivalent sets so that the density of internal states ρ_{int} to be used in eqs 4.1 and 4.7 is quite similar for both reactions.

Second, as explained in Section 7.A, both the ion−dipole and ion−quadrupole electrostatic potentials lead to an asymptotic adiabatic separation and hence to a common constraint $\varepsilon^{1/2}$. For both interactions, the dynamical factor of the MEM is expected to be $\exp(-\lambda_1\varepsilon^{1/2})$, in conformity with the low-energy experimental findings.

Third, the Lagrange multiplier λ_1 must be positive for the following reason. Within the ion−neutral potential well, all oscillators may be assumed to nearly (but not completely) freely exchange energy. They are therefore in a state of quasi-equilibrium and may be characterized by a common effective temperature,[1,67] Because the ion−neutral complex in reactions 1.1 or 1.2 dissociates without any reverse activation barrier, the potential energy increases steadily, and the effective temperature decreases as fragmentation proceeds. As the reaction coordinate reaches large values, it decouples from the bath formed by the other degrees of freedom. The entropy deficiency derives from this decoupling. The reaction coordinate now tends to form a closed subsystem, where the total energy is constant. As a result, the effective temperature reached at the end of the fragmentation process will be smaller for the relative translation than for the internal degrees of freedom. Therefore, the translational energy necessarily decreases with respect to the reference statistical situation, where a common effective temperature would govern all degrees of freedom. In the language of the MEM, $\lambda_1 > 0$, and the measured translational energy release $\langle\varepsilon\rangle$ must be less than the statistical expectation. This accounts for the experimental findings.

C. Role of Long-Range Forces. Let us now compare the $C_4H_4^+ + C_2H_2$ and $C_4H_4^+ +$ HCN dissociation channels. The ion−dipole complex is found to be more stable than the ion−quadrupole one (0.53 eV versus 0.14 eV, according to the ab initio calculations presented in Section 6). A deep potential well induces a strong cooling in the reaction coordinate and a strong discrepancy between the final effective temperature for the relative translation and that for the internal degrees of freedom of the fragments. This correlates with the experimental data. In the spirit of Section 7.B, the Klots equation[1,67] may be slightly modified by assigning a different effective temperature to the relative translation and to the remaining degrees of freedom. Both effective temperatures can then be easily extracted from the experimental average translational energy and from the complementary average fragment internal energy, respectively. In the 0−3 eV total energy range, the ratio between the fragment translational effective temperature and that for the internal degrees of freedom is 0.93 ± 0.07 for the benzene dissociation. In the pyridine case, this ratio decreases to 0.78 ± 0.10. These data show that, especially for reaction 1.2, the relative translation contributes more to the conversion of kinetic energy into potential energy along the dissociation path than

the vibrotational bath, a situation which is compatible with the progressive decoupling of the reaction coordinate from the remaining degrees of freedom. Coming back to the MEM language, one must therefore have, at a given internal energy, $\lambda_1^{pyr} > \lambda_1^{bz}$ and $\langle\varepsilon\rangle^{pyr}/\langle\varepsilon\rangle_0^{pyr} < \langle\varepsilon\rangle^{bz}/\langle\varepsilon\rangle_0^{bz}$. This accounts for the differences between Panels a and b of Figure 4.

D. Dimensionality of the Dynamics. In order to analyze the influence of anisotropy of the long-range potential, it is useful to compare our results with those previously derived in a case where the interaction potential between fragments is spherically symmetric.[40] In that case, that is, when it can be expressed as the sum of an ion−induced-dipole interaction and a centrifugal term, the conservation of the orbital angular momentum in a central force field constrains the relative motion of the two fragments to take place in a plane.[57,66] Then, the two-dimensional prior distribution $P_{2D}^0(\varepsilon|E)$ (eq 4.7) is found to provide an excellent approximation to the experimental KERD. The only necessary additional correction consists in truncating it at low values of ε, because of the additional requirement that the translational energy be large enough to overcome the centrifugal barrier.[1,40]

The argument based on the conservation of the orbital angular momentum breaks down when the interaction potential is anisotropic. Surprisingly enough, the experimental data for reaction 1.1 are close to the two-dimensional prior expectations. This observation arouses the presumption that, for nonobvious reasons, the nuclear trajectories that generate the KERD for reaction 1.1 have a propensity to be confined to a two-dimensional space even though the interaction potential is not spherically symmetric.

The use of eq 4.7 as a two-dimensional prior distribution that satisfies the conservation of angular momentum has been advocated by Quack and Troe.[68] It must be emphasized, however, that evaluating the correction linked with the truncation at low values of ε is far from straightforward because the calculation of the barrier height requires the assumption that the total angular momentum can be decomposed into two decoupled momenta, rotational and orbital. This is impossible in a nonrigid system.[69] This is the reason why we carried out our MEM analysis with the more secure three-dimensional prior distribution.

Instead, we propose to analyze the classical Hamiltonian of a model system. Consider the interaction between an ion of mass M and a diatomic molecule consisting of two masses m separated by a distance $2d$. The nine degrees of freedom are reduced to five by fixing the origin of the coordinates at the center of mass of the whole system and by freezing the internuclear distance d. For the five remaining degrees of freedom, we use a double system of spherical coordinates (Figure 6): the distance r separating the ion and the center of mass of the diatomic molecule, the polar and azimuth angles ω and φ denoting the orientation of that segment, and the polar and azimuth angles ξ and η specifying the orientation of the diatomic. The following expression can be derived for the kinetic energy:[57,70]

$$T = \frac{1}{2\mu}\left(p_r^2 + \frac{p_\omega^2}{r^2} + \frac{p_\varphi^2}{r^2 \sin^2 \omega}\right) + \frac{1}{2I}\left(p_\xi^2 + \frac{p_\eta^2}{\sin^2 \xi}\right) \quad (7.4)$$

where $\mu = 2\ mM/(M + 2m)$ denotes the reduced mass of the two fragments and $I = 2md^2$ is the moment of inertia of the diatomic molecule.

Expression 7.4 is valid for both reactions 1.1 and 1.2 if we accept to reduce C_2H_2 and HCN to a rigid diatomic molecule. This should be acceptable at large values of r and at energies low enough for the neutral fragment to retain a rigid structure.

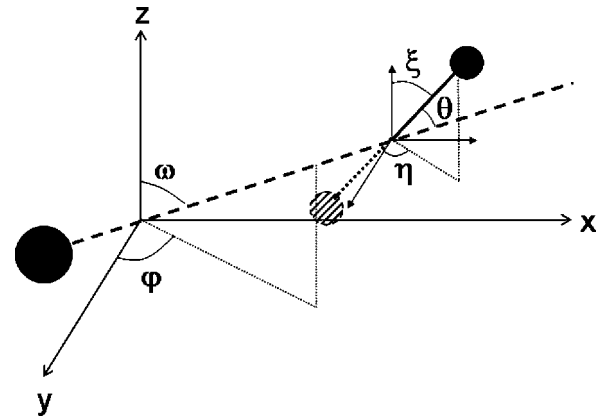

Figure 6. Definition of the coordinate system used for the classical Hamiltonian analysis of the atom−diatom model of Section 7.D.

The expression of the potential energy results from inserting the following standard formula into eqs 7.1 or 7.2:

$$\cos\theta = \cos\omega\cos\zeta + \sin\omega\sin\zeta\cos(\eta - \varphi) \quad (7.5)$$

The important point is that the Hamiltonian involves five momenta but only four generalized coordinates: r, ω, ξ, and the difference $\eta - \varphi$. Thus, one of the coordinates is cyclic, and as a result, it is possible to define a generalized momentum that is a constant of the motion.

To see this explicitly, let us define a new angle $\delta = \eta - \varphi$. The kinetic energy can be rewritten as

$$T = \frac{1}{2\mu}\left(p_r^2 + \frac{p_\omega^2}{r^2} + \frac{(p_\varphi - p_\delta)^2}{r^2 \sin^2 \omega}\right) + \frac{1}{2I}\left(p_\xi^2 + \frac{p_\delta^2}{\sin^2 \xi}\right) \quad (7.6)$$

The gratifying result is that φ vanishes from the expression of the potential energy because

$$\cos\theta = \cos\omega\cos\zeta + \sin\omega\sin\xi\cos\delta \quad (7.7)$$

The angle φ is now a cyclic (or ignorable) coordinate.[57,70] Thus, its conjugate momentum p_φ is a constant of the motion in addition to the energy. The relative translational motion of the pair of fragments is described in spherical coordinates by the three variables r, ω, and φ. If the latter degree of freedom is now frozen, the translational phase-space volume is reduced to two dimensions, both for the ion−dipole and ion−quadrupole interactions. More explicitly, the translational phase space volume is determined by integration over three coordinates (r, ω, φ) but over the two variable conjugate momenta (p_r and p_ω) only. Each integration over a momentum increases the exponent of ε by 1/2, whereas each integration over a coordinate leaves it unchanged.[1] Thus, the translational phase-space volume is proportional to ε, and its derivative, that is, the density of states, is a constant. This justifies the use of the two-dimensional prior distribution $P_{2D}^0(\varepsilon|E)$ in the MEM analysis and accounts for the lowering of the experimental translational energy with respect to the statistical expectation.

That the charge−quadrupole interaction exerts only a weak influence on the orbital motion should not be too surprising. Its main effect is to create a precession of the quadrupole about an axis perpendicular to the orbital plane. This result has an astronomical analogy because of the similarity between the electrostatic and the gravitational potentials. As a matter of fact, because of its rotation, the Earth is an oblate spheroid and therefore presents a gravitational quadrupole moment.[57] Its equatorial bulge induces a torque that leads to a precession of the rotational axis about the normal to the ecliptic (termed the

precession of the equinoxes) but which does not prevent the Earth's orbit from remaining planar.

8. Concluding Remarks

Previous research has shown that virtually all of the dissociations with no reverse barrier present a KERD typical of a two-dimensional interfragment motion. The present paper has attempted to explain why this is the case. Insight into the problem comes from the introduction of the concept of adiabatic separation of the reaction coordinate and from an understanding of the mechanism leading to a dimensionality reduction of the translational degrees of freedom.

The central theme of this work is the comparison between the KERDs characterizing reactions 1.1 and 1.2, including the perdeuterated species. The reaction mechanism consists of a complicated sequence of rearrangements leading to an ion−dipole or ion−quadrupole complex that dissociates without any reverse activation energy. Our measurements and calculations shed light on the last step only, that is, on the dissociation of the weakly bound species. A major finding is that in all of these reactions, less translational energy is released than what is statistically expected.

The asymptotic part of the potential energy surface of the molecular ion thus governs the KERDs for all these reactions: long-range forces are instrumental. Do then the KERDs reveal the specificity of theses forces? Hardly. This paradox is in fact only apparent. The KERD shapes of reactions 1.1 and 1.2 are alike because the corresponding long-range potentials have, in spite of their dissimilarity, an essential common feature: they both lead to an adiabatic separation of the reaction coordinate. The validity of this adiabatic approximation is demonstrated by the experimental observation that the KERDs for both reactions are related to $P^0_{3D}(\varepsilon|E)$ with the momentum $\varepsilon^{1/2}$ acting as a constraint. This is a consequence of Jacobi's version of the least-action principle.

On the other hand, the KERD has been shown to be simply related to $P^0_{2D}(\varepsilon|E)$ whenever the interaction potential is simple enough to depend only on a number of angles less than the originally required set. When this reduction is valid, a cyclic variable appears in the Hamiltonian, and its conjugate momentum is a constant of the motion. A reduction of the number of translational degrees of freedom has often been suggested in the rationalization of unimolecular reaction dynamics,[1] but we believe the argument developed in Section 7.D to be more straightforward.

The question may be raised whether there exists a connection between the concepts of adiabatic separability and variational principle, which lead to the $\exp(-\lambda_1\varepsilon^{1/2})$ correction, on one side, and the reduction to two translational dimensions, on the other side. Additional work is beyond doubt required to reach a deeper understanding. We suggest that such a link might be found in Gauss's variational principle of least constraint[71] applied to the case of a charge−dipole interaction. Among three possible trajectories, a linear one, a planar one, and a gauche one, it can be shown that the planar one happens to minimize the constraint.

These two simplifications, adiabatic separability and dimensionality reduction of the translational phase space, apply to all ion−molecule reactions where a diatomic-like fragment separates from a point-like entity. These circumstances are very general and can be expected to be applicable to the dissociation of the numerous ion−neutral complexes and weakly bound species that have been detected in the chemistry of gas−phase ions.[72−74]

Finally, attention should be drawn to an unexpected conclusion, derived from the invariance properties of the entropy. Although the analytical expression of the dynamical constraint identified by the MEM analysis of our experimental KERDs is linked to the properties of the electrostatic potential in the asymptotic range of the reaction coordinate (eqs 7.1 ans 7.2), its influence persists throughout the entire reaction process. Alhassid and Levine[75] have analytically demonstrated that the entropy deficiency is a constant of motion, and this is also supported by quantum dynamical calculations of reactive scattering.[76] This means that the influence of the constraint subsists at smaller values of the reaction coordinate, in particular in the ion−neutral complex, where it prevents the oscillators to completely freely exchange their energy, as already alluded to in Section 7.B. Thus, in contradistinction to summary sketches of the RRKM theory, the system never forgets its previous history. The analytical expression of the constraint for an ion−molecule reaction is simple and involves only the reaction coordinate when $r \rightarrow \infty$. However, it becomes more complicated and less conspicuous at shorter distances where many degrees of freedom can be affected, so that the restrictions to phase-space sampling and to energy randomization act everywhere along the reaction coordinate.

References and Notes

(1) Baer, T.; Hase, W. L. *Unimolecular Reaction Dynamics. Theory and Experiments*; Oxford University Press: New York, 1996.
(2) Forst, W. *Unimolecular Reactions. A concise Introduction*; Cambridge University Press: Cambridge, 2003.
(3) Gilbert, R. G.; Smith, S. C. *Theory of Unimolecular and Recombination Reactions*; Blackwell Scientific Publications: Oxford, UK, 1990.
(4) Lorquet, J. C.; Leyh, B. Statistical theories in mass spectrometry. In *The Encyclopedia of Mass Spectrometry*; Armentrout, P. B., Ed.; Elsevier: Amsterdam, 2003; Vol. 1.
(5) Laskin, J.; Lifshitz, C. *J. Mass Spectrom.* **2001**, *36*, 459.
(6) Leyh, B.; Lorquet, J. C. Kinetic energy release distributions in mass spectrometry. In *The Encyclopedia of Mass Spectrometry*; Armentrout, P. B., Ed.; Elsevier: Amsterdam, 2003; Vol. 1.
(7) Leyh, B.; Gridelet, E.; Locht, R.; Lorquet, J. C. *Int. J. Mass Spectrom.* **2006**, *249*, 250–330.
(8) Lorquet, J. C. *Int. J. Mass Spectrom.* **2000**, *200*, 43.
(9) Gridelet, E.; Locht, R.; Lorquet, A. J.; Lorquet, J. C.; Leyh, B. *Int. J. Mass Spectrom.* **2003**, *228*, 389.
(10) Levine, R. D.; Bernstein, R. B. Thermodynamic Approach to Collision Processes. In *Dynamics of Molecular Collisions, Part B*; Miller, W. H., Ed.; Plenum: New York, 1976; pp 323.
(11) Levine, R. D.; Kinsey, J. L. Information-Theoretic Approach: Application to Molecular Collisions. In *Atom-Molecule Collision Theory. A Guide for the Experimentalist*; Bernstein, R. B., Ed.; Plenum: New York, 1979; pp 693.
(12) Levine, R. D. *Adv. Chem. Phys.* **1981**, *47*, 239.
(13) Urbain, P.; Remacle, F.; Leyh, B.; Lorquet, J. C. *J. Phys. Chem.* **1996**, *100*, 8003.
(14) Urbain, P.; Leyh, B.; Remacle, F.; Lorquet, A. J.; Flammang, R.; Lorquet, J. C. *J. Chem. Phys.* **1999**, *110*, 2911.
(15) Gridelet, E.; Locht, R.; Lorquet, A. J.; Lorquet, J. C.; Leyh, B. *J. Phys. Chem. A* **2006**, *110*, 8519.
(16) Fati, D.; Lorquet, A. J.; Locht, R.; Lorquet, J. C.; Leyh, B. *J. Phys. Chem. A* **2004**, *108*, 9777.
(17) Urbain, P.; Leyh, B.; Remacle, F.; Lorquet, J. C. *Int. J. Mass Spectrom.* **1999**, *185/186/187*, 155.
(18) Baer, T.; Willett, G. D.; Smith, D.; Phillips, J. S. *J. Chem. Phys.* **1979**, *70*, 4076.
(19) Jarrold, M. F.; Wagner-Redeker, W.; Illies, A. J.; Kirchner, N. J.; Bowers, M. T. *Int. J. Mass Spectrom. Ion Proc.* **1984**, *58*, 63.
(20) Kühlewind, H.; Kiermeier, A.; Neusser, H. J. *J. Chem. Phys.* **1986**, *85*, 4427.
(21) Kühlewind, H.; Kiermeier, A.; Neusser, H. J.; Schlag, E. W. *J. Chem. Phys.* **1987**, *87*, 6488.
(22) Kiermeier, A.; Kühlewind, H.; Neusser, H. J.; Schlag, E. W.; Lin, S. H. *J. Chem. Phys.* **1988**, *87*, 6488.
(23) Grebner, T. L.; Neusser, H. J. *Int. J. Mass Spectrom Ion Proc.* **1999**, *185/186/187*, 517.
(24) van der Hart, W. J. *Int. J. Mass Spectrom. Ion Proc.* **1998**, *176*, 23.

(25) Staley, S. W.; Norden, T. D. *J. Am. Chem. Soc.* **1989**, *111*, 445.
(26) Hoxha, A.; Locht, R.; Lorquet, A. J.; Lorquet, J. C.; Leyh, B. *J. Chem. Phys.* **1999**, *111*, 9259.
(27) Barber, M.; Elliot, R. M. *12th Annual Conference on Mass Spectrometry and Allied Topics*, 1964, Montreal.
(28) Jennings, K. R. *J. Chem. Phys.* **1965**, *43*, 4176.
(29) Barber, M.; Green, B. N.; Wolstenholme, W. A.; Jennings, K. R. *Adv. Mass Spectrom.* **1968**, *4*, 89.
(30) Cooks, R. G.; Beynon, J. H.; Caprioli, R. M.; Lester, G. R. *Metastable Ions*; Elsevier: Amsterdam, 1973.
(31) Holmes, J. L.; Osborne, A. D. *Int. J. Mass Spectrom. Ion Phys.* **1977**, *23*, 189.
(32) Rumpf, B. A.; Derrick, P. J. *Int. J. Mass Spectrom. Ion Proc.* **1988**, *82*, 239.
(33) Yeh, I. C.; Kim, M. S. *Rapid Commun. Mass Spectrom.* **1992**, *6*, 115.
(34) Moon, J. H.; Choe, J. C.; Kim, M. S. *J. Phys. Chem. A* **2000**, *104*, 458.
(35) Chupka, W. A. Photoionization and fragmentation of polyatomic molecules. In *Chemical Spectroscopy and Photochemistry in the Vacuum Ultraviolet*; Sandorfy, C., Ausloos, P. J., Robin, M. B., Eds.; NATO Advanced Study Institutes, Reidel: Boston, 1974; Series C, Vol. 8.
(36) Neusser, H. J. *J. Phys. Chem.* **1989**, *93*, 3897.
(37) Klippenstein, S. J.; Faulk, J. D.; Dunbar, R. C. *J. Chem. Phys.* **1993**, *98*, 243.
(38) Holland, D. M. P.; Shaw, D. A.; Sumner, I.; Bowler, M. A.; Mackie, R. A.; Shpinkova, L. G.; Cooper, L.; Rennie, E. E.; Parker, J. E.; Johnson, C. A. F. *Int. J. Mass Spectrom.* **2002**, *220*, 31.
(39) Hoxha, A.; Leyh, B.; Locht, R. *Rapid Commun. Mass Spectrom.* **1999**, *13*, 275.
(40) Gridelet, E.; Lorquet, J. C.; Leyh, B. *J. Chem. Phys.* **2005**, *122*, 094106.
(41) Eland, J. H.; Berkowitz, J.; Schulte, H.; Frey, R. *Int. J. Mass Spectrom. Ion Phys.* **1978**, *28*, 297.
(42) Rosenstock, H. M.; Stockbauer, R.; Parr, A. C. *Int. J. Mass Spectrom. Ion Phys.* **1981**, *38*, 323.
(43) Lifshitz, C. *J. Phys. Chem.* **1982**, *86*, 606.
(44) Lifshitz, C.; Malinovich, Y. *Int. J. Mass Spectrom Ion Proc.* **1984**, *60*, 99.
(45) Arakawa, R.; Arimura, M.; Yoshikawa, Y. *Int. J. Mass Spectrom. Ion Proc.* **1985**, *64*, 227.
(46) Arakawa, R.; Yoshikawa, Y. *Bull. Chem. Soc. Jpn.* **1987**, *60*, 49.
(47) Burgers, P. C.; Holmes, J. L.; Mommers, A. A.; Szulejko, J. E.; Terlouw, J. K. *Org. Mass Spectrom.* **1984**, *19*, 442.
(48) Zhang, M. Y.; Carpenter, B. K.; McLafferty, F. W. *J. Am. Chem. Soc.* **1991**, *113*, 9499.
(49) Lias, S. G.; Bartmess, J. E.; Liebman, J. F.; Holmes, J. L.; Levin, R. D.; Mallard, W. G. *J. Phys. Chem. Ref. Data* **1988**, *17*, Supplement no. 1.
(50) Urena, F. P.; Gomez, M. F.; Gonzales, J. J. L.; Torres, E. M. *Spectrochim. Acta* **2003**, *A 59*, 2815.
(51) Lin, M. F.; Dyakov, Y. A.; Tseng, C. M.; Mebel, A. M.; Lin, S. H.; Lee, Y. T.; Ni, C. K. *J. Chem. Phys.* **2005**, *123*, 054309.
(52) Locht, R.; Leyh, B.; Jochims, H. W.; Baumgärtel, H. unpublished.
(53) Hrouda, V.; Roeselova, M.; Bally, T. *J. Phys. Chem. A* **1997**, *101*, 3925.
(54) Koster, G.; van der Hart, W. J. *Int. J. Mass Spectrom. Ion Proc.* **1997**, *163*, 81.
(55) Iachello, F.; Levine, R. D. *Europhys. Lett.* **1987**, *4*, 389.
(56) Levine, R. D. *Adv. Chem. Phys.* **1988**, *70*, 53.
(57) Goldstein, H.; Poole, C.; Safko, J. *Classical Mechanics*; Addison Wesley: San Francisco, 2002.
(58) Frisch, M. J.; Trucks, G. W.; Schlegel, H. B.; Scuseria, G. E.; Robb, M. A.; Cheeseman, J. R.; Montgomery, J. A., Jr.; Vreven, T.; Kudin, K. N.; Burant, J. C.; Millam, J. M.; Iyengar, S. S.; Tomasi, J.; Barone, V.; Mennucci, B.; Cossi, M.; Scalmani, G.; Rega, N.; Petersson, G. A.; Nakatsuji, H.; Hada, M.; Ehara, M.; Toyota, K.; Fukuda, R.; Hasegawa, J.; Ishida, M.; Nakajima, T.; Honda, Y.; Kitao, O.; Nakai, H.; Klene, M.; Li, X.; Knox, J. E.; Hratchian, H. P.; Cross, J. B.; Bakken, V.; Adamo, C.; Jaramillo, J.; Gomperts, R.; Stratmann, R. E.; Yazyev, O.; Austin, A. J.; Cammi, R.; Pomelli, C.; Ochterski, J. W.; Ayala, P. Y.; Morokuma, K.; Voth, G. A.; Salvador, P.; Dannenberg, J. J.; Zakrzewski, V. G.; Dapprich, S.; Daniels, A. D.; Strain, M. C.; Farkas, O.; Malick, D. K.; Rabuck, A. D.; Raghavachari, K.; Foresman, J. B.; Ortiz, J. V.; Cui, Q.; Baboul, A. G.; Clifford, S.; Cioslowski, J.; Stefanov, B. B.; Liu, G.; Liashenko, A.; Piskorz, P.; Komaromi, I.; Martin, R. L.; Fox, D. J.; Keith, T.; Al-Laham, M. A.; Peng, C. Y.; Nanayakkara, A.; Challacombe, M.; Gill, P. M. W.; Johnson, B.; Chen, W.; Wong, M. W.; Gonzalez, C.; Pople, J. A. *Gaussian 03*, revision B.04; Gaussian, Inc.: Wallingford, CT, 2004.
(59) Jensen, F. *Introduction to computational chemistry*; Wiley: Chichester, 1999.
(60) Andersson, S.; Grüning, M. *J. Phys. Chem. A* **2004**, *108*, 7621.
(61) Bates, D. R. *Chem. Phys. Lett.* **1981**, *82*, 396.
(62) Kern, K.; Schlier, C. *Z. Phys. D* **1986**, *1*, 391.
(63) Lorquet, J. C. *J. Phys. Chem. A* **2007**, *111*, 8050.
(64) Lorquet, J. C. *Int. J. Quantum Chem.* **2008**, *108*, 1629.
(65) Pavlov-Verevkin, V. B.; Lorquet, J. C. *J. Chem. Phys.* **2005**, *123*, 074324/1.
(66) Corben, H. C.; Stehle, P. *Classical Mechanics*; Wiley: New York, 1950.
(67) Klots, C. E. *J. Chem. Phys.* **1973**, *58*, 5364.
(68) Quack, M.; Troe, J. Statistical methods in scattering. *Theoretical Chemistry: Advances and Perspectives*; Academic Press: New York, 1981; Vol. 6B, p 199.
(69) Chapuisat, X.; Nauts, A.; Durand, G. *Chem. Phys.* **1981**, *56*, 91.
(70) Landau, L. D.; Lifshitz, E. M. *Mechanics*; Pergamon Press: Oxford, 1960.
(71) Whittaker, E. T. *A Treatise on the Analytical Dynamics of Particles and Rigid Bodies*; Cambridge University Press: Cambridge, 1988.
(72) Bowen, R. D. *Acc. Chem. Res.* **1991**, *24*, 364.
(73) McAdoo, D. J.; Morton, T. H. *Acc. Chem. Res.* **1993**, *26*, 295.
(74) Grützmacher, H. F. *Int. J. Mass Spectrom Ion Proc.* **1992**, *118/119*, 825.
(75) Alhassid, Y.; Levine, R. D. *J. Chem. Phys.* **1977**, *67*, 4321.
(76) Nesbet, R. K. Surprisal theory. *Theoretical Chemistry: Advances and Perspectives*; Academic Press: New York, 1981; Vol. 6B, p 79.

JP8033424